crystals

MDPI

Article

X-ray Single-Crystal Analysis, Pharmaco-Toxicological Profile and Enoyl-ACP Reductase-Inhibiting Activity of Leading Sulfonyl Hydrazone Derivatives

Yoanna Teneva [1], Rumyana Simeonova [1], Orlin Besarboliev [2], Hristina Sbirkova-Dimitrova [3] and Violina T. Angelova [1,*]

[1] Faculty of Pharmacy, Medical University of Sofia, 1000 Sofia, Bulgaria; yoanna.koedzhikova@gmail.com (Y.T.); rsimeonova@pharmfac.mu-sofia.bg (R.S.)
[2] Institute of Emergency Medicine "N. I Pirogov", Bul. Totleben 21, 1000 Sofia, Bulgaria; or.basarboliev@gmail.com
[3] Institute of Mineralogy and Crystallography "Acad. Ivan Kostov", Bulgarian Academy of Sciences, Acad. G. Bonchev Street, Bl. 107, 1113 Sofia, Bulgaria; hsbirkova@gmail.com
* Correspondence: v.stoyanova@pharmfac.mu-sofia.bg

Abstract: Taking into consideration the growing resistance towards currently available antimycobacterials, there is still an unmet need for the development of new chemotherapeutic agents to combat the infectious agents. This study presents X-ray single-crystal analysis to verify the structure of leading sulfonyl hydrazone **3b**, which has proven its potent antimycobacterial activity against *Mycobacterium tuberculosis* H37Rv with an MIC value of 0.0716 μM, respectively, low cytotoxicity, and very high selectivity indexes (SI = 2216), and which has been fully characterized by Nuclear Magnetic Resonance (NMR) and High-Resolution Mass Spectrometry (HRMS) methods. Furthermore, this study assessed the ex vivo antioxidant activity, acute and subacute toxicity, and in vitro inhibition capacity against enoyl-ACP reductase of hydrazones **3a** and **3b**, as **3a** was identified as the second leading compound in our previous research. Compared to isoniazid, compounds **3a** and **3b** demonstrated lower acute toxicity for intraperitoneal administration, with LD_{50} values of 866 and 1224.7 mg/kg, respectively. Subacute toxicity tests, involving the repeated administration of a single dose of the test samples per day, revealed no significant deviations in hematological and biochemical parameters or pathomorphological tissues. The compounds exhibited potent antioxidant capabilities, reducing malondialdehyde (MDA) levels and increasing reduced glutathione (GSH). Enzyme inhibition assays of the sulfonyl hydrazones **3a** and **3b** with IC_{50} values of 18.2 μM and 10.7 μM, respectively, revealed that enoyl acyl carrier protein reductase (InhA) could be considered as their target enzyme to exhibit their antitubercular activities. In conclusion, the investigated sulfonyl hydrazones display promising drug-like properties and warrant further investigation.

Keywords: tuberculosis; sulfonyl hydrazones; acute toxicity; sub-acute toxicity; antioxidant activity; *Mycobacterium tuberculosis*; enoyl-ACP reductase; single crystal X-ray diffraction

Citation: Teneva, Y.; Simeonova, R.; Besarboliev, O.; Sbirkova-Dimitrova, H.; Angelova, V.T. X-ray Single-Crystal Analysis, Pharmaco-Toxicological Profile and Enoyl-ACP Reductase-Inhibiting Activity of Leading Sulfonyl Hydrazone Derivatives. *Crystals* **2024**, *14*, 560. https://doi.org/10.3390/cryst14060560

Academic Editor: Tom Leyssens

Received: 21 May 2024
Revised: 4 June 2024
Accepted: 11 June 2024
Published: 17 June 2024

1. Introduction

Despite the advancement in drug discovery over the last two decades, tuberculosis (TB) remains a global health challenge, with a reported incidence during 2021 of 10.6 million new cases and an increased incidence of multidrug-resistant/rifampicin-resistant TB (MDR/RR-TB) between 2020 and 2021 (with an estimated 450,000 new cases in 2021) [1]. Another unfavorable finding is that the COVID-19 pandemic had a detrimental impact on the dynamics of the disease. Therefore, due to the continuous and rising resistance towards the currently applied antimycobacterial agents and the high cost and prolonged duration of MDR/RR-TB treatment regimens, the discovery of novel

non-toxic drug candidates with straightforward mechanisms of action has emerged as highly important.

Meanwhile, sulfonyl hydrazones were reported to possess a variety of pharmacological effects, including antimycobacterial [2–5] and antimicrobial [3,6–9] effects, in numerous literature sources.

Based on the literature findings, our scientific group focused their work on sulfonyl hydrazone moiety as a potent antimycobacterial scaffold. In a previous publication of our scientific unit during 2022, we described the preparation and characterization of a series of novel sulfonyl hydrazones [10]. Their antimycobacterial activity was assessed against Mycobacterium tuberculosis strain H37Rv and cytotoxicity was evaluated against two cell lines (HEK-293T and CCL-1), ADME/Tox computational predictions were undertaken, and they were successfully docked with two crystallographic structures of enoyl-ACP reductase (InhA), providing encouraging insights into their potential mechanisms of action. Among the series, sulfonyl hydrazones **3a** and **3b** testified significant antitubercular activity, expressed in the lowest values of MIC—0.0763 and 0.0716 μM—and the highest selectivity indexes—1819 and 2216, respectively [10]. Their chemical scaffolds are presented in Figure 1.

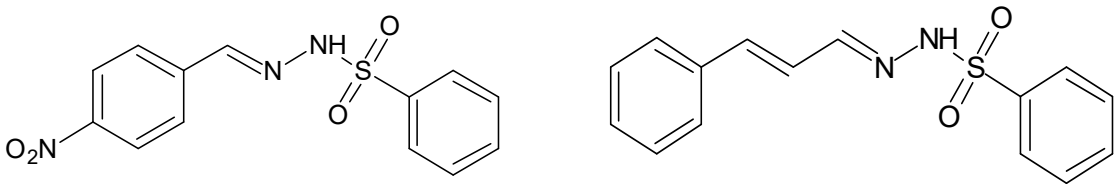

Figure 1. (**a**) Chemical structure of **3a**; (**b**) chemical structure of **3b**.

In another study by our research group, we reported the in vivo toxicity, redox-modulating capacity, and intestinal permeability of antimycobacterial aroyl hydrazone derivatives containing thiadiazole and indole fragments [11]. Also, in connection with the future prospects of our work, we performed a detailed review on the recent advances in antimycobacterial hydrazide-hydrazones, which inhibit the InhA enzyme [12].

Consequently, in continuation of our previously initiated work with sulfonyl hydrazones [10], the aim of the present study is to evaluate the toxicological effect of the two lead compounds (**3a** and **3b** on Figure 1), when administered to experimental animals, to assess their potential antioxidant activity and to further examine their potential mechanisms of action by inhibiting the enzyme enoyl-ACP reductase (InhA), which was suggested by the results of the molecular docking with crystallographic structures of the enzyme.

2. Material and Methods

2.1. Chemistry

The chemicals and reagents used in the preparation of the compounds were purchased from Sigma-Aldrich (Merck KGaA, Darmstadt, Germany).

N′-[(4-nitrophenyl)methylidene]benzenesulfonohydrazide (**3a**) was prepared by a condensation reaction of p-nitrobenzaldehyde and benzenesulfonohydrazide, while N′-[3-phenylprop-2-en-1-ylidene]benzenesulfonohydrazide (**3b**) was prepared by a condensation reaction of cinnamaldehyde and benzenesulfonohydrazide at a molar ratio 1:1 (4.0 mmol) in absolute ethanol for 1–3 h, as described before [10]. The two synthesized derivatives were confirmed by ^{1}H and ^{13}C nuclear magnetic resonance (NMR), and high-resolution mass spectrometry (HRMS) data [10]. The spectral characteristics are presented in Table S1 (Supplementary Information).

2.2. Biology

2.2.1. Experimental Animals

This study protocol has been approved by the Animal Care Ethics Committee, and additionally the Bulgarian Agency for Food Safety issued ethical clearance for the study (No. 125, from 7 October 2020). The mice were housed, maintained, and euthanized in accordance with the applicable international guidelines, outlined in the European Convention for the Protection of Vertebrate Animals used for Experimental and Other Scientific Purposes (ETS 123) [13].

The study Involved male and female pathogen-free Jcl: ICR mice, aged 6 weeks and weighing 25–30 g. These mice were sourced from the National Breeding Center in Sofia, Bulgaria. A minimum acclimatization period of 7 days was observed before the study initiated. Throughout the 14-day experimental period, the mice had access to age-appropriate standard complete commercial pelleted mouse feed and fresh drinking water ad libitum. The animals were kept in Plexiglas cages, with four animals per cage, following a 12/12 h light/dark cycle under standard laboratory conditions. The ambient temperature was maintained at 20 ± 2 °C, and humidity was kept at 72 ± 4%. In the acute toxicity test, 54 female mice were used, while 32 male mice were involved in the sub-acute toxicity test. Prior to the experiment, the mice underwent a seven-day acclimatization period in the vivarium, during which their health was monitored daily.

2.2.2. Acute Toxicity in Mice

The study assessed the acute toxicity of the compounds in 54 female mice using both peroral (p.o.) and intraperitoneal (i.p.) administration. The assessment followed a simplified version of the Lorke method, with minor adjustments. The method allows substances to be ranked and classified according to the Globally Harmonised System for chemical classification [14]. We used three animals per dose at 5 fixed doses. For both compounds, during the p.o. route of administration, the lowest dose was 500 mg/kg and the highest dose was 5000 mg/kg. During the i.p. route, the lowest dose for both compounds was 250 mg/kg and the highest was 1500 mg/kg b.w. Both compounds were solubilized with Tween 80 (0.1%) before application due to low water solubility. We calculated the LD_{50} by means of the following equation, $LD_{50} = \sqrt{D_0 \times D_{100}}$, where D_0 is the highest non-lethal dose and D_{100} is the lowest lethal dose [15]. In the study, surviving animals were closely monitored during the initial 24 h, with observations conducted every 3 h. Subsequently, daily observations were made for up to 14 days. On the 14th day, the animals were anesthetized using ketamine/xylazine, followed by decapitation and thorough examination of the internal organs for any potential macroscopic abnormalities, including assessments related to organ color, consistency, and the presence of neoplasms.

2.2.3. Sub-Acute Toxicity in Mice

To make assessments of the sub-acute toxicity of the two investigated compounds, they were administered intraperitoneally for 14 days to male mice. The two studied derivatives were administered to animals in two concentrations, calculated as 1/20 and 1/10 from the LD_{50} value, received after i.p. administration during the acute toxicity study. For **3a**, the two doses were 45 mg/kg and 90 mg/kg body weight, while for **3b** the doses were 65 mg/kg and 130 mg/kg b.w. In the study, male Jcl: ICR mice aged 6 weeks and weighing approximately 40–45 g were used. The substances were administered daily via intraperitoneal (i.p.) injection for a duration of 14 days, with consistent timing each day. To facilitate administration, the compounds were solubilized in a solution containing Tween 80 (0.1%) in distilled water. The injection volume was 0.1 mL per 10.0 g of body weight. Throughout the study, the animals were closely monitored for behavioral changes and signs of toxicity. Positive control isoniazid (INH) was used for a comparison of all results.

2.2.4. Experimental Design

For the sub-acute toxicity tests, the animals were divided into 6 experimental groups, each consisting of 6 mice (n = 6):

Group 1—control, untreated group;
Group 2—mice treated i.p. with isoniazid (INH) 50 mg/kg [16];
Group 3—mice treated i.p. with **3a** at a dose of 45 mg/kg (1/20 LD_{50});
Group 4—mice treated i.p. with **3a** at a dose of 90 mg/kg (1/10 LD_{50});
Group 5—mice treated i.p. with **3b** at a dose of 65 mg/kg (1/20 LD_{50});
Group 6—mice treated i.p. with **3b** at a dose of 130 mg/kg (1/10 LD_{50}).

During the study, the body weights of the treated animals were measured on days 1, 5, 7, 11, and 13 using a laboratory balance. On the 14th day, the animals received anesthesia of ketamine and xylazine, followed by decapitation. Blood samples for serum biochemical investigations were collected in tubes containing a clot activator. After centrifugation at 3000× *g* for 10 min, the serum was separated. Additionally, blood was taken in vacutainers after decapitation for a complete blood count, which was assessed using an automated biochemical analyzer (BS-120, Mindray, China) following the manufacturer's instructions. The following hematological parameters were measured—white blood cells (WBC), lymphocytes (LYM), hemoglobin (HgB), hematocrit (HCT), and platelets (PLT)—following the manufacturer's instructions for a semi-automated hematological analyzer BC-2800 Vet, (Mindray, Shenzhen, China). Livers were extracted to perform an assessment of the biomarkers of oxidative stress influence. Additionally, livers and kidneys were preserved for pathomorphological analysis.

2.2.5. Histological Evaluation of Tissue Specimens

After euthanizing the mice, tissues from the liver and kidneys were collected and fixed in 10% buffered formalin for 48 h. The fixed tissues underwent processing using the classic paraffin method [17]. Subsequently, paraffin blocks were cut using a paraffin rotary microtome (Leica RM 2255, Wetzlar, Germany) at a slice thickness of 5 µm. Hematoxylin and eosin (H&E, Surry Hills, Australia) staining was performed on the sections. Finally, histological changes were examined and imaged using a Leica DM2500 (Wetzlar, Germany) light microscope equipped with both a Leica MC120HD digital camera (Wetzlar, Germany) and a Euromex BioBlue digital camera (Arnhem, The Netherlands).

2.3. Assessment of the Oxidative Stress Biomarkers

In this specific study, the researchers assessed oxidative stress levels by quantifying thiobarbituric acid reactive substances (TBARS). This was achieved by assessing the amount of malondialdehyde (MDA) equivalents, following the method steps described by Polizio and Peña [18]. Additionally, an examination of the non-protein sulfhydryls after protein precipitation with trichloroacetic acid (TCA), outlined in the approach of Bump et al. [19], was applied to determine the amount of reduced glutathione (GSH).

Catalase activity was examined by the application of the method of Aebi et al. [20]. The CAT activity was studied by assessing the breakdown of H_2O_2. During this process, the decrease in absorbance at 240 nm was monitored spectrophotometrically using a Spectro UV-VIS Split Beam (Labomed, Inc., Los Angeles, CA, USA) during the decomposition of H_2O_2. The molar extinction coefficient of 0.043 mM^{-1} cm^{-1} was used to calculate enzyme activity, which was expressed as nM/min/mg protein.

2.4. InhA Inhibition Assay

The in vitro InhA inhibition activity of the compounds was studied by means of the spectrophotometric method, as previously reported by Chetty et al. [21] and Doğan et al. [22,23] with slight modifications. All necessary reagents and the recombinant *Mycobacterium tuberculosis* enoyl-[acyl-carrier-protein] reductase were purchased from Sigma-Aldrich (Merck KgaA, Darmstadt, Germany). The investigated compounds were studied in five different concentrations—1 µM, 10 µM, 25 µM, 50 µM, and 100 µM. Triclosan was used

as a positive control at concentration. All solid compounds were dissolved in DMSO at a concentration of 1 mg/mL and diluted to the necessary concentrations, i.e., the concentration of DMSO in the final assay was not higher than 1%. The final volume of each sample was 1 mL, containing 30 nM Pipes buffer, 250 µM NADH, 50 µM trans-2-dodecenoyl-coenzyme A, 220 nM InhA, and the solution of the investigated compound. The absorbance was measured at 340 nm using Spectro UV-VIS Split Beam (Labomed, Inc.) apparatus, measuring the oxidation of NADH to NAD+ for one minute. The control sample contained all described components, except for the inhibitor. All assays were performed in triplicate. For calculation of the % enzyme inhibition, initial velocity (v) was calculated for the first minute from the slope of the plot absorbance vs. time for each concentration. The initial velocity of the control reaction without inhibitor (v0) was also estimated. The % inhibition activity of the compounds was calculated from formulate $[1 - (v/v0)] \times 100$, where v/v0 is the residual activity of the enzyme. The IC_{50} values were calculated by plotting the % enzyme inhibition vs. the logarithm of inhibitor's concentration.

2.5. Single-Crystal X-ray Analysis

In this study, diffraction data were received at 150 K using the ω-scan technique. A Bruker D8 Venture diffractometer equipped with a PhotonII CMOS detector was employed, utilizing mirror-monochromatized Mo Kα radiation from a micro-focus source (λ = 0.7107 Å). The determination of cell parameters, data integration, scaling, and absorption correction was performed using Bruker Apex 4 and Saint and Sadabs program packages [24,25]. The structures were solved through intrinsic methods using SHELXT [26] and refined by full matrix least-square procedures on F2 (SHELXL) [26]. Non-hydrogen atoms were refined anisotropically, while hydrogen atoms were placed at idealized positions and refined using the riding model. Notably, the hydrogen atom near N1 was located from a difference Fourier map and refined freely. The fundamental crystal and refinement data are presented in Table S2 (Supplementary Information) in a summarized format.

The structural analysis crystallographic data (excluding structure factors) were deposited with the Cambridge Crystallographic Data Centre, CCDC No. 2356559. A copy of this information may be obtained free of charge from The Director, CCDC, 12 Union Road, Cambridge CB2 1EZ, UK. 06/01/2024 Fax: +44-1223-336-033, e-mail: deposit@ccdc.cam.ac.uk, or www.ccdc.cam.ac.uk, accessed on 21 May 2024.

3. Results and Discussion

3.1. Synthesis of the Sulfonyl Hydrazone Derivatives

The preparation of sulfonyl hydrazones by a condensation reaction (Figure 2) has been described previously in detail [10]. The two derivatives, which are the subject of the current study, demonstrated significant results—lowest MICs, low cytotoxicity and highest selectivity index—and are presented in Figure 1. The spectral characteristics are presented in Table S1 (Supplementary Information).

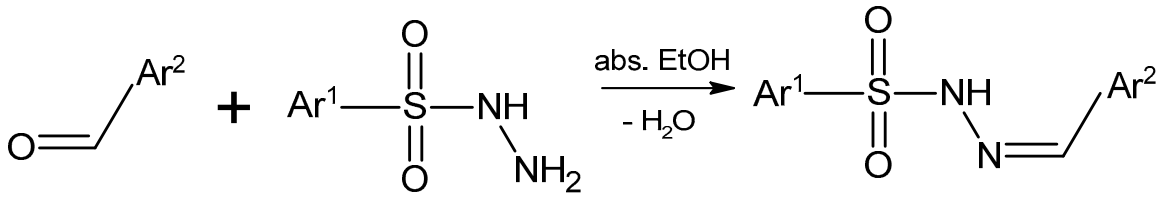

3a: Ar^1 = phenyl; Ar^2= *p*-nitrophenyl

3b: Ar^1 = phenyl; Ar^2= 3-phenylprop-2-en-1-yl

Figure 2. Synthetic procedure for the preparation of the sulfonyl hydrazones.

3.2. X-ray Crystallography

We were able to grow single crystals of **3b** suitable for structural analyses by slow evaporation from a mixture of hexane/diethyl ether (3:1). Compound **3b** crystallizes in the monoclinic space group $P2_1/c$ (No 4) with one molecule per asymmetric unit (Figure 3) and four molecules in the unit cell (Z = 4). The refinement of the structure showed that the molecular features of **3b** (bond distances and angle, Tables S3–S5, Supplementary Information) are similar to those of analogical compounds [27–30]. The molecule in the crystal structure adopts the (*E*,*E*) conformation. The 3-phenylprop-2-en-1-yl (Ar^2 moiety) is nearly planar, with *rmsd* of the mean plane 0.071 Å (Figure 4a). The angle between the two aromatic rings is 82.83°, and thus adjacent molecules are "head to tail" oriented. One typical hydrogen bond (N1–H1...O3) and two weak C–H...O interactions (Table 1) stabilize the three-dimensional arrangement of the molecules in the crystal structure of **3b** (Figure 4b). As a result, pseudo-layers, produced through chains with $C_1^1(4)$ graph set notation, are visualized along *ab* (Figure 5).

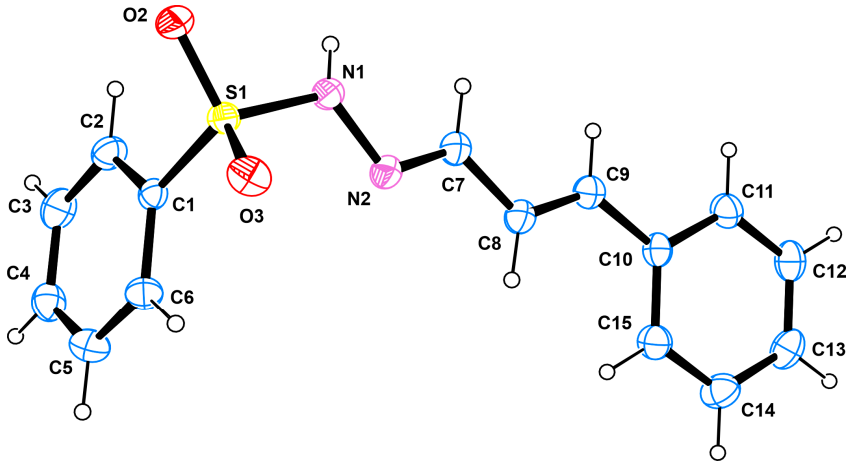

Figure 3. Molecular structure of **3b**, as obtained by single-crystal X-ray structural analysis (50% ellipsoids; H atoms are shown as spheres of arbitrary radii).

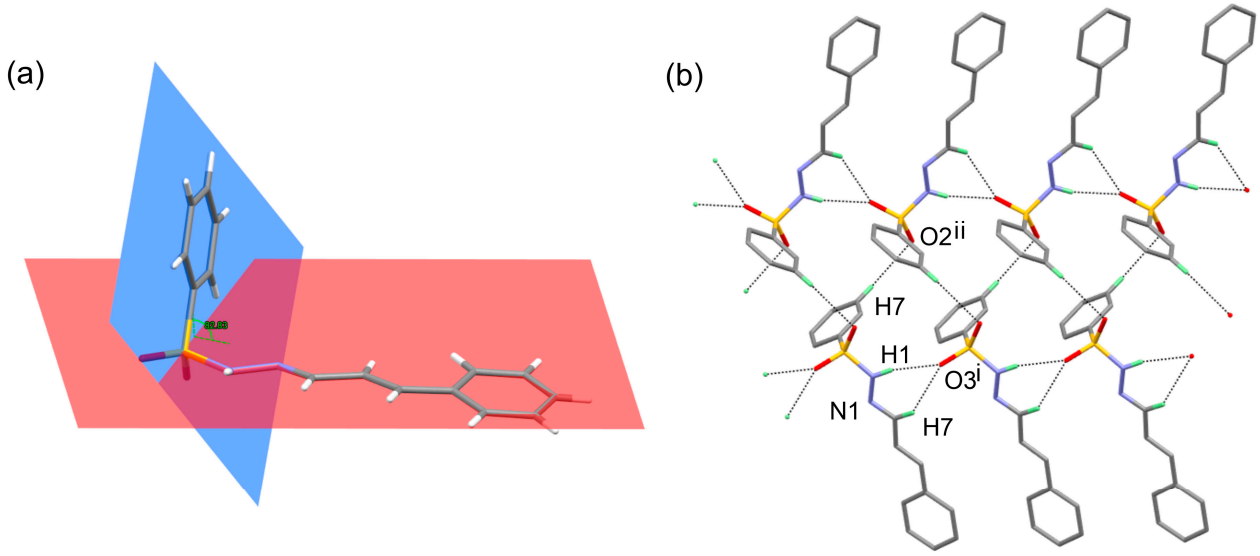

Figure 4. Depiction of (**a**) the angle between the mean planes of Ar2 and Ar1 and (**b**) the visualization of the hydrogen bond and weak C–H...O interactions (indicated by dashed lines) between adjacent molecules of **3b**; symmetry operation: (i) x, 1 + y, z; (ii) 2 − x, y − 1/2, 3/2 − z.

Table 1. Acute intraperitoneal toxicity of **3a**.

Dose mg/kg b.w.	Effect/Lethality	Time of Occurrence	Symptoms
1500	2/3 (66%)	After 24 h	Delayed reflexes, somnolence, lethal outcome
1000	1/3 (33%)	After 7 days	Impaired coordination, rapid breathing, lethal outcome
750	0/3	-	-
500	0/3	-	-
250	0/3	-	-

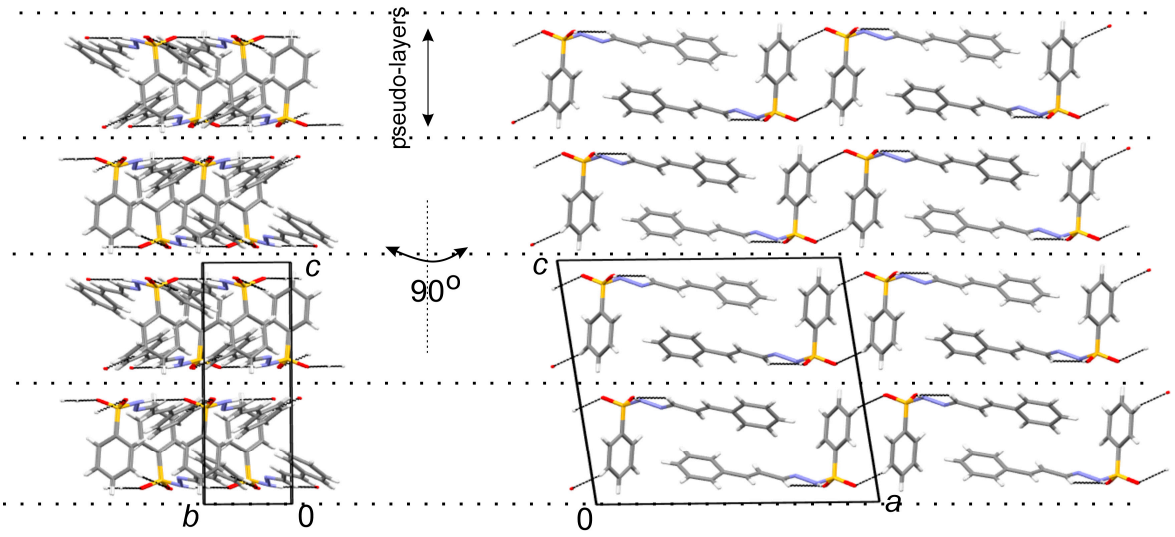

Figure 5. Crystal packing diagram of **3b**, viewed along a and b axes (the hydrogen bonds are indicated by dashed lines) disclosing the formation of pseudo layers.

3.3. Acute Toxicity in Mice

During the oral toxicity study, the highest administered dose for both compounds was 5000 mg/kg and no mortality was associated with it, which may be a result of the poor resorption of the studied substances. The results from the i.p. toxicity tests of the two derivatives are presented in Tables 1 and 2.

Table 2. Acute intraperitoneal toxicity of **3b**.

Dose mg/kg b.w.	Effect/Lethality	Time of Occurrence	Symptoms
1500	3/3 (100%)	After 24 h	Respiratory failure with long pauses, ataxia, piloerection, seizures, lethal outcome.
1000	0/3	-	-
750	0/3	-	-
500	0/3	-	-
250	0/3	-	-

Based on the results from the above table, for **3a**, D_0 is 750 mg/kg, D_{100} is 1000 mg/kg, and $LD_{50} = \sqrt{D_0 \times D_{100}} = \sqrt{750 \times 1000} = 866$ mg/kg.

As a result of the conducted study, no lethality occurred within the oral administration at the highest dose of 5000 mg/kg, and therefore LD_{50} is calculated as >3000 mg/kg. The resorption index (IR) is then calculated as follows:

$$IR = LD_{50}\ \text{i.p.}/LD_{50}\ \text{p.os.} \times 100 = 866/3000 \times 100 \approx 28.9\%$$

Based on the above, for **3b**, D_0 is 1000 mg/kg, D_{100} is 1500 mg/kg, and $LD_{50} = \sqrt{D_0 \times D_{100}} = \sqrt{1000 \times 1500} = 1224.7$ mg/kg.

Also, no mortality occurred within oral administration at the highest dose of 5000 mg/kg for **3b**, as well, and LD_{50} was calculated as >3000 mg/kg. IR is then calculated as follows:

$$IR = LD_{50}\ \text{i.p.}/LD_{50}\ \text{p.os.} \times 100 = 1224.7/3000 \times 100 \approx 40.8\%$$

The study of the acute toxicity of the two novel sulfonyl hydrazones resulted in them showing low oral toxicity and slightly more expressed parenteral toxicity. According to the Hodge and Sterner scale [31], the two leading sulfonyl derivatives could be classified as slightly toxic after oral and intraperitoneal administration to female mice, as LD_{50} is in the range of 500–5000 mg/kg. A more in-depth analysis shows that **3a** demonstrated slightly higher toxicity compared to **3b**, due to the fact that at a concentration of 1000 mg/kg b.w. **3a** led to 33% mortality, while at the same dose, the other derivative led to no mortality. The **3b** exhibited its toxic effect at a dose of 1500 mg/kg.

3.4. Sub-Acute Toxicity of Mice, Hematological and Biochemical Parameters, and Markers of Oxidative Stress after the Sub-Acute Toxicity Study

As described in Section 2, Materials and Methods, during the sub-acute toxicity tests, the two investigated compounds were administered intraperitoneally at approximately the same time every day for 14 continuous days. Changes in the body weight of the experimental animals are presented in Figures 6 and 7.

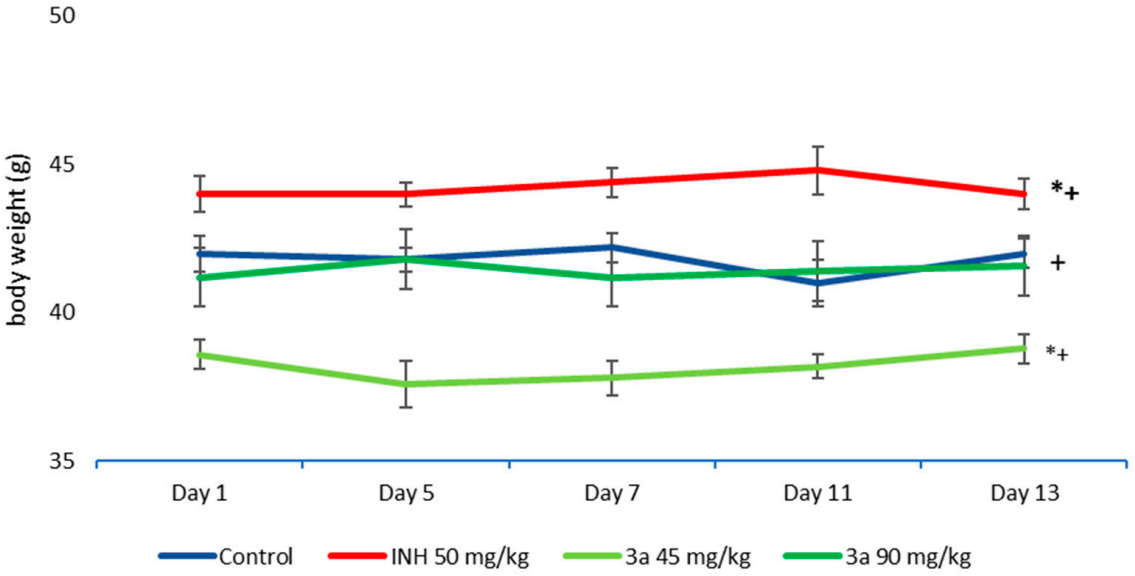

Figure 6. Changes in body weight of animals treated with INH and **3a** in comparison to control group; * $p \leq 0.05$ vs. control group; $^+$ $p \leq 0.05$ vs. INH group. Results are presented as mean ± SD (n = 6).

During the 14-day experimental period, the administration of INH, **3a** 45 mg/kg, and **3b** in both doses resulted in statistically significant alterations in the body weight ($p \leq 0.05$). All six groups of animals showed slight weight changes during different stages of the experiment. However, a more detailed review of the results might demonstrate that **3b** in both concentrations of 65 mg/kg and 130 mg/kg led to a slight weight gain in treated animals, compared to the body weight on the first day of the experiment. The assumption of our scientific group is that this might be related to the cinnamon scaffold in the structure of **3b**, as there are literature sources testifying a slight appetite-enhancing effect of trans-cinnamaldehyde [32].

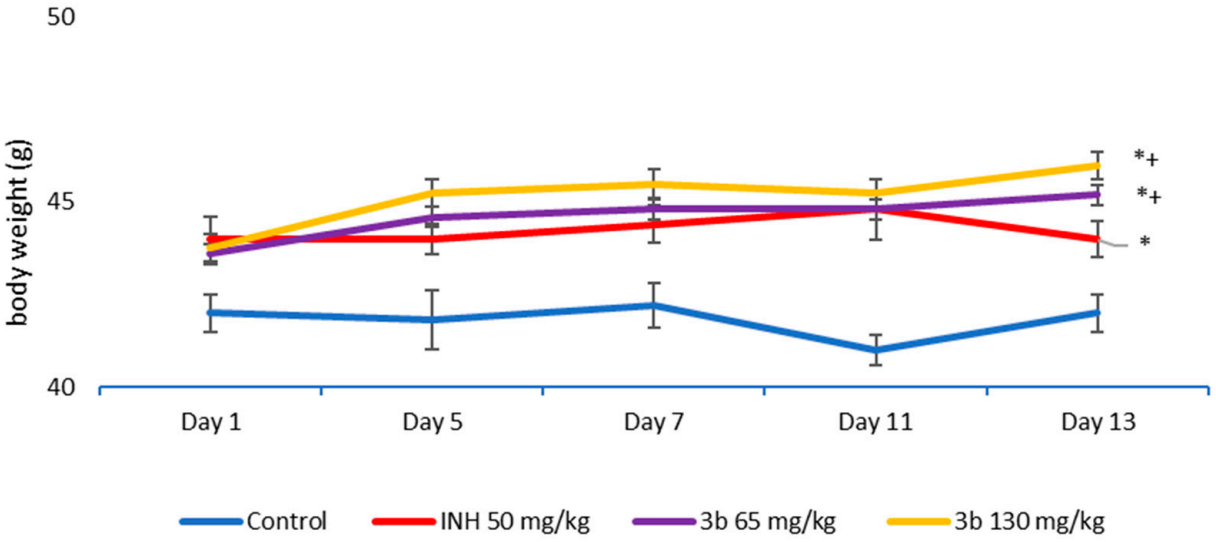

Figure 7. Changes in body weight of animals treated with INH and **3b** in comparison to control group; * $p \leq 0.05$ vs. control group; $^{+}$ $p \leq 0.05$ vs. INH group. Results are presented as mean ± SD (n = 6).

3.5. Complete Blood Count (CBC) and Biochemistry in the Blood of Mice

The complete blood count of the treated animals is presented in Table S7, while Table S8 summarizes the results from biochemistry tests run on both plasma and blood serum. Both tables are present in the Supplementary Information Material. A more in-depth analysis of the received results has been conducted and showed that both studied compounds at each of their doses led to a slight decrease in the levels of lymphocytes and erythrocytes in comparison to the control group, although the levels still remained within the reference values interval. Increased levels of blood glucose and urea were demonstrated by all treated groups, including INH-administered animals, in comparison to the controls, in Table S8 in the Supplementary Information. However, the testified values remain mainly within the reference value range. During the experiment, there were no deviations outside the reference values reported in literature sources for the particular breeds of animals.

3.6. Markers of Oxidative Stress

In our investigation, we explored the pharmacological characteristics of both sulfonyl hydrazones and their toxicity mechanisms. Specifically, we focused on the impact of ROS-mediated homeostasis in the liver of experimental animals. Lipid peroxidation, which occurs in cellular biomembranes, is most commonly mediated by free radical processes. The measurement of MDA content (endogenous genotoxic product) is typically employed as a basis for determining the level of lipid peroxidation and reflecting the extent of tissue and cell damage caused by prooxidant agents [33].

As illustrated in Figure 8, the 14-day intraperitoneal administration of INH and the higher doses of both compounds increased the level of MDA by 26.5%, 16.9%, and 9.6%, respectively, compared to the control group. However, in the animals treated with both compounds and at both administered doses, the level of MDA was statistically significantly lower than in the group treated with isoniazid. In the groups treated with the low doses **3a** and **3b**, the level of MDA was 32% and 33% lower compared to the INH group and was practically comparable to that of the control animals.

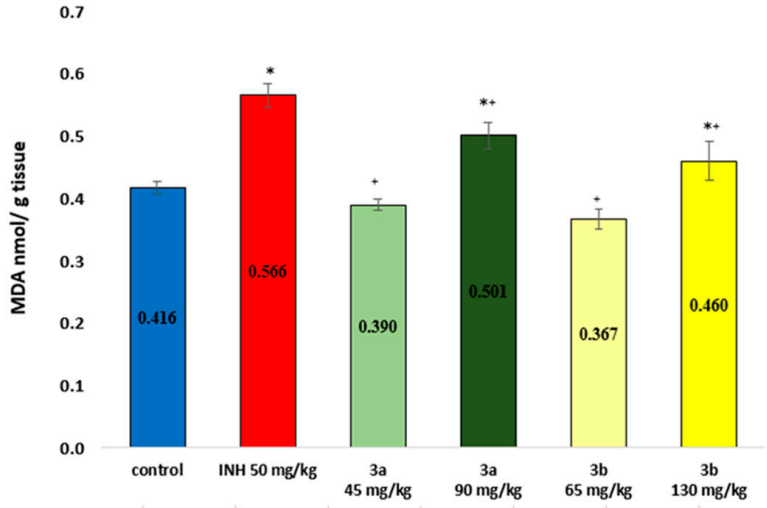

Figure 8. Endogenous content of MDA in the liver homogenate of experimental groups. The significance of the data was assessed using the nonparametric Mann–Whitney U test. Results are presented as mean ± SD (n = 6 for each compound and dose). * $p \leq 0.05$ vs. control group; $^{+}$ $p \leq 0.05$ vs. INH group.

The most crucial redox modulator that regulates inflammatory processes in the body is glutathione (GSH), and it is usually referred to as a "master antioxidant". It plays a vital role in maintaining cellular health by neutralizing reactive oxygen species (ROS) and supporting antioxidant defenses [34]. Liver diseases, triggered by factors such as drugs, alcohol, diet, and environmental pollutants, often disrupt GSH normal levels [35]. Also, glutathione depletion occurs if ROS production is not controlled, and this leads to increased patient susceptibility to immunosuppression, organ damage, increased vascular permeability, shock, and thrombotic events [36]. The conduction of an endogenous GSH content test led to the results presented in Figure 9. Isoniazid and the two tested compounds in both doses led to a statistically significant decrease in the level of GSH compared to the control group. INH decreased the level of GSH by 76%, which was statistically significant; low doses of the two studied compounds reduced the level of GSH by about 62%, and high doses of **3a** and **3b** decreased the level of GSH by 43% and 30%, respectively, compared to the control group. Both compounds administered at both doses reduced the depletion of GSH, and it was statistically higher compared to isoniazid. In the group treated with compound **3a**, the GSH levels were 37.3% and 57.3%, respectively, higher than in INH-treated animals, while in the groups treated with compound **3b** the level of GSH was 36.7% and 65.5% higher than in the INH group.

Catalase is an essential antioxidant enzyme that plays a critical role in extenuating oxidative stress to a considerable level. Its effect is achieved by breaking down cellular hydrogen peroxide into water and oxygen. When catalase is deficient or malfunctions, it is associated with the pathogenesis of several age-related degenerative diseases, including diabetes mellitus, hypertension, anemia, vitiligo, Alzheimer's disease, Parkinson's disease, bipolar disorder, cancer, and schizophrenia [37]. As demonstrated in Figure 10, the repeated administration of compound **3a** at a concentration of 90 mg/kg led to a statistically significant increase in the level of catalase, by 25.9% and 33.1% in comparison to the control and the INH group. Derivative **3b** statistically significantly increased the activity of catalase by 15.3% and 30% vs. the control group and by 23.5% and 36.8% in comparison to the INH group. This increase in the activity of the enzyme is probably related to the attempt of the liver tissue to overcome the oxidative stress and liver damage caused by compound **3b**, and this liver disorder was also evident in the histomorphology observations (see below in Figure 12e,f).

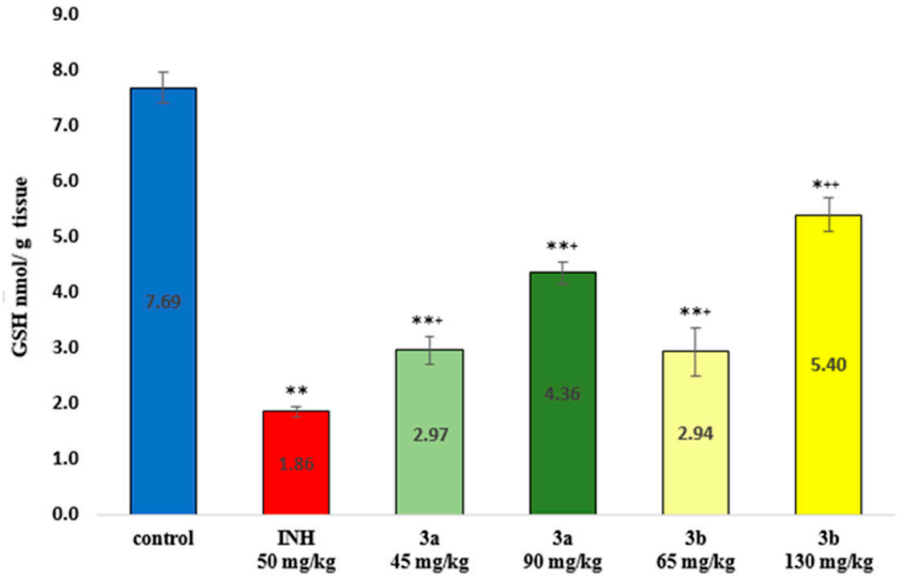

Figure 9. Endogenous content of GSH in the liver homogenate of experimental groups. The significance of the data was assessed using the nonparametric Mann–Whitney *U* test. Results are presented as mean ± SD (n = 6 for each compound and dose). ** $p \leq 0.01$ vs. control group; $^{+}$ $p \leq 0.05$ vs. INH group. The notation "** $p \leq 0.01$ vs. control group" indicates a statistically significant difference between a treatment group and a control group. p ≤ 0.01 means that the probability of observing the difference between a treatment group and a control group by chance is less than or equal to 1%. The notation "$^{+}$ $p \leq 0.05$ vs. INH group" means that there is a statistically significant difference between the group being compared and the INH (isoniazid) group. Specifically, $p \leq 0.05$ indicates that the probability of observing the difference between these groups by chance is less than or equal to 5%. The symbols ** and $^{+}$ show in the diagram for which results are valid the statistically significant differences.

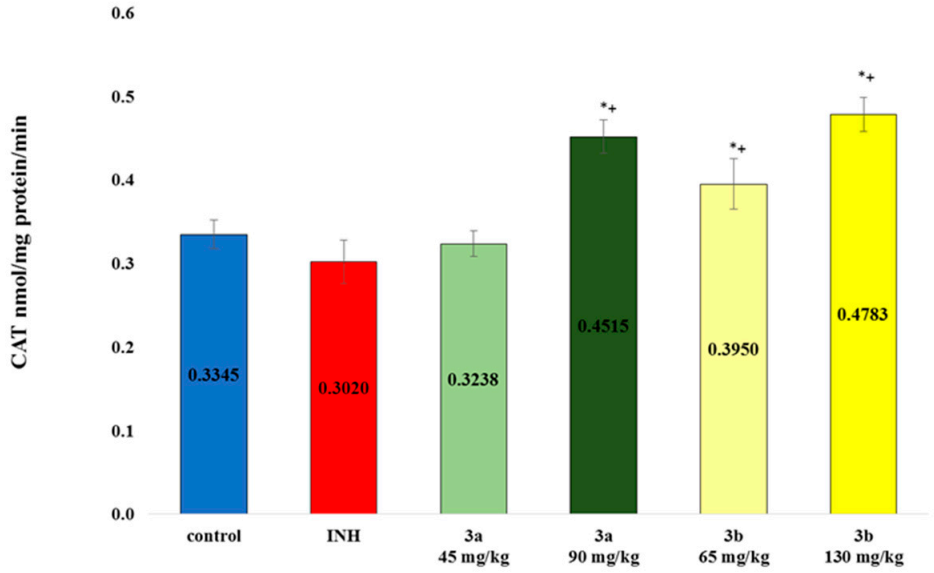

Figure 10. Activity of catalase enzyme in the liver homogenate of experimental groups after sub-acute toxicity study. The significance of the data was assessed using the nonparametric Mann–Whitney U test. Results are presented as mean ± SD (n = 6 for each compound and dose). * $p \leq 0.05$ vs. control group; $^{+}$ $p \leq 0.05$ vs. INH group.

3.7. Histological Examination of Tissue Specimens Post-Mortem

3.7.1. Kidneys

Histological findings in the kidneys show normal histology without pathological deviations (Figure 11). There are small foci of lymphocytic infiltration in the parenchyma. Vascular congestion without intimal hyperplasia and obliteration of the lumens was observed. No signs of tubular atrophy, inflammation and glomerulitis were present. The tubules were lined with epithelium with a preserved histologic structure. Elements of glomerular and extraglomerular mesangium were visualized with no proliferation. The renal pelvis in all tested groups had normal architecture.

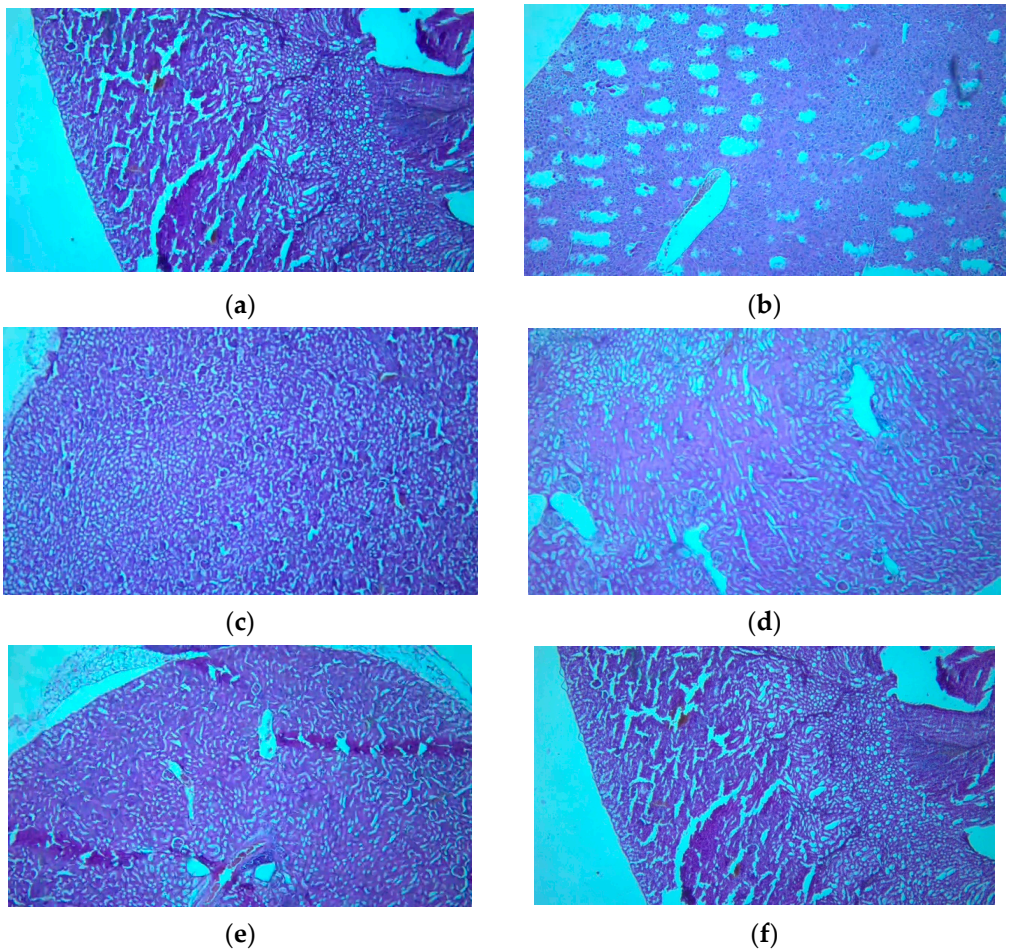

Figure 11. Pathomorphological findings in the kidneys in mice after intraperitoneal administration of INH and investigated compounds. Legend: (**a**) control group—not treated; (**b**) INH 50 mg/kg; (**c**) **3a** 45 mg/kg; (**d**) **3a** 90 mg/kg; (**e**) **3b** 65 mg/kg; (**f**) **3b** 130 mg/kg b.w. The field magnification is 100×.

3.7.2. Liver

The histological findings in the liver parenchyma showed isolated degenerative changes. The overall architecture was preserved with lobular configuration and an absence of major remodeling changes. Areas of cholestasis were present in all groups. Vascular congestion, minimal periportal (predominantly lymphocytic) inflammation and the dilation of sinusoidal spaces were observed. Signs of increased ballooning degeneration in small percentages of hepatocytes in groups **3b** 65 mg/kg and **3b** 130 mg/kg were found. In these two groups, areas of necrosis were present measuring, respectively, 0.1 cm and 0.3 cm. The areas of necrosis are circled in red in Figure 12.

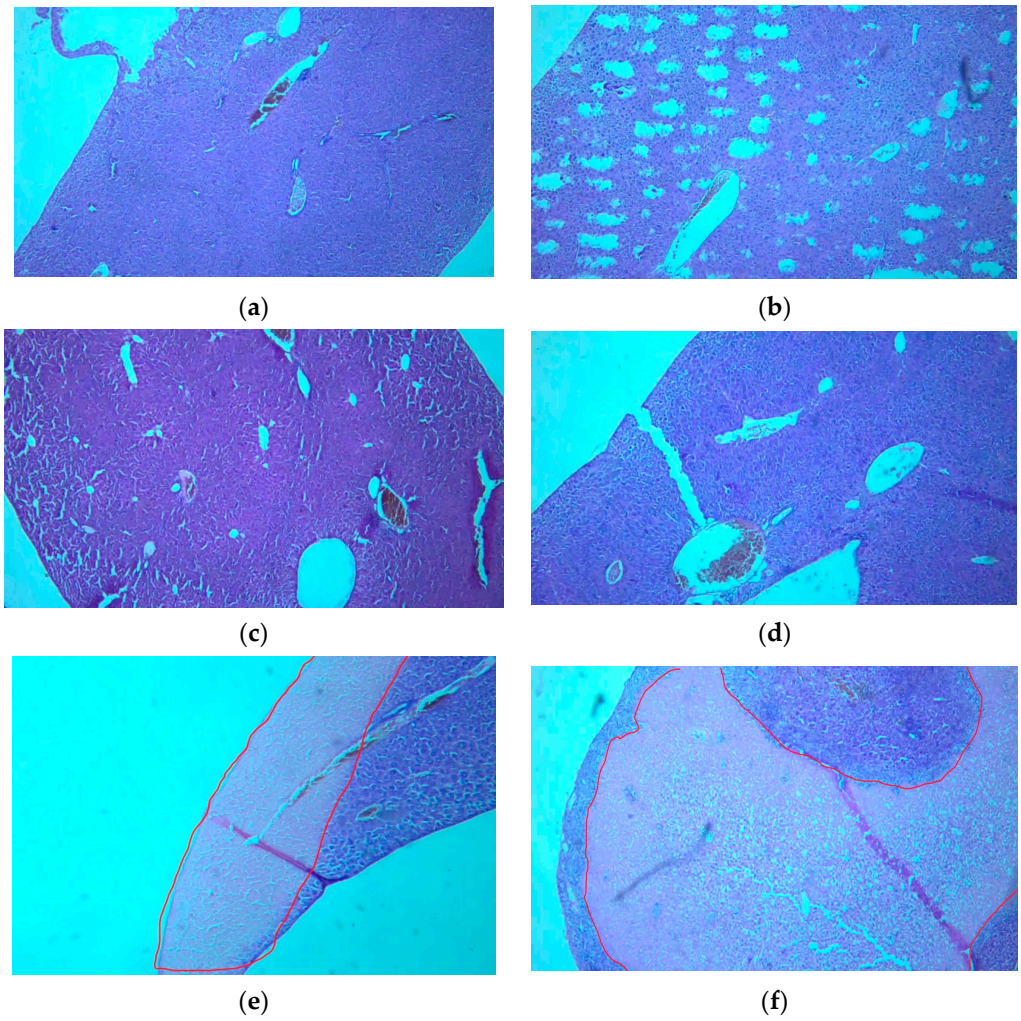

Figure 12. Pathomorphological findings in the liver in mice after intraperitoneal administration of INH and investigated compounds. Legend: (**a**) control group—not treated; (**b**) INH 50 mg/kg; (**c**) **3a** 45 mg/kg; (**d**) **3a** 90 mg/kg; (**e**) **3b** 65 mg/kg; (**f**) **3b** 130 mg/kg. The field magnification is 100×.

3.8. In Vitro InhA Inhibition Assay

In a previous publication by our scientific unit, molecular docking of the sulfonyl hydrazones **3a** and **3b** with two X-ray crystallographic structures of *M. tuberculosis* enoyl reductase (PDB ID 2X22 and PDB ID 4TZK) was reported [10]. The results of the molecular docking showed that **3b** appeared as the top-ranked compound after docking with both structures of InhA with scores of −12.36 and −12.83 kcal/mol, while **3a** presented slightly lower docking scores of −11.98 and −12.80 kcal/mol, presenting the protein–ligand interaction (PLI) diagrams of the sulfonyl hydrazones **3a** and **3b** in the ligand-binding domains of both receptors, 2X22 and 4TZK. In both enzyme structures, the reference compound isoniazid recorded worse results, with docking scores of −9.18 and 8.51 [10]. Encouraged by the outcome of the molecular docking study, an in vitro InhA inhibition assay was conducted to confirm whether the enoyl-ACP reductase can be validated as one of the targets of the investigated derivatives. The results of the spectrophotometrically conducted assay of the potential enoyl-ACP reductase inhibition effect demonstrated that both compounds possess a moderate to good inhibition activity, slightly higher than 50%. The inhibition capacity of each concentration of the investigated compounds is presented in Table 3. Triclosan (TCS) was used as a positive reference compound, as a broad-spectrum antibacterial agent commonly found in personal care products. The average inhibition activity of compound **3a** has been calculated as 57.8%; for compound **3b**, the average inhibition activity was

calculated as 53.1%, while the sample, containing triclosan, demonstrated 82.3% inhibition activity against the recombinant *Mycobacterium tuberculosis Mtb* enoyl-acyl carrier protein reductase enzyme at the particular reaction conditions. Compound **3a** at a concentration of 100 μM demonstrated equal activity to the positive control triclosan at the same concentration. By plotting the percentage inhibition against each concentration for the two compounds, the IC_{50} values were calculated as 18.2 μM and 10.7 μM for compounds **3a** and **3b**, respectively. The results received during the InhA inhibition assay provide potential pharmacological pathways to combatting the resistance of *Mycobacterium tuberculosis* (*Mtb*) towards izoniazid and other first-line options. Considering that the enzyme inhibition values are consistent with the antimycobacterial activity of the compounds and the previously reported results from molecular docking with two crystallographic structures of InhA [10], it can be concluded that the inhibition of the enoyl-ACP reductase enzyme is a validated pathway for the activity of these compounds.

Table 3. InhA inhibition capacity of the two investigated compounds at each of their concentrations.

Compound	Concentration (μM)	Initial Velocity of Reaction	% Inhibition of InhA
3a	1	0.0009	35.2
	10	0.0006	54.1
	25	0.0006	52.9
	50	0.0005	64.7
	100	0.0002	82.3
3b	1	0.0009	29.3
	10	0.0006	54.1
	25	0.0006	58.8
	50	0.0005	64.7
	100	0.0006	58.8
Triclosan	100	0.0002	82.3

4. Conclusions

To conclude, in the current study, the investigated sulfonyl hydrazones **3a** and **3b** were characterized for their acute oral and intraperitoneal toxicity; sub-acute intraperitoneal toxicity in mice; influence on the biomarkers of oxidative stress; and in vitro enoyl-ACP reductase inhibition activity. Additionally, the structure of the leading compound **3b** was elucidated using single-crystal X-ray diffraction. In the crystal structure, the molecule adopts the (*E*,*E*) conformation. In the in vivo investigations, enzymatic activities and varying pH levels can influence their stereochemistry, which is a limitation of the study and could be taken into account in further studies. The tested compounds were classified as slightly toxic, according to the Hodge and Sterner scale, and have good tolerability from the experimental animals, do not lead to any statistically significant deviations in biochemical and hematological parameters, and show only isolated pathomorphological deviations. The repeated administration of compound **3b** led to a slight weight gain in the treated animals, which might be related to the cinnamon fragment in its structure, which has been described to show a low appetite-enhancing effect in some literature sources. In addition, the two derivatives demonstrated moderate InhA inhibition capacity during the in vitro experiment with recombinant *Mtb* InhA reductase enzyme. To conclude, the two chemical compounds possess the necessary characteristics to be considered for further development as drugs to help in combatting the ongoing resistance of *Mycobacterium tuberculosis* towards isoniazid and other first-line therapies.

Supplementary Materials: The following supporting information can be downloaded at: https://www.mdpi.com/article/10.3390/cryst14060560/s1, Table S1. Spectral characteristics of **3a** and **3b**; Table S2. Crystal data and structure refinement for **3b**; Table S3. Bond Lengths for **3b**; Table S4. Bond Angles for **3b**; Table S5. Torsion Angles for **3b**; Table S6. Hydrogen Bonds for **3b**; Table S7. Hematological parameters (HP) after 14 day admin-istration of INH, **3a** and **3b**; Table S8. Biochemical parameters (BP) of INH and sulfonyl hydra-zones **3a** and **3b**.

Author Contributions: Conceptualization, V.T.A. and R.S.; writing—original draft preparation, writing—review and editing, Y.T., R.S. and V.T.A.; supervision, R.S. and V.T.A.; project administration, R.S. and V.T.A.; funding, Y.T. and V.T.A.; Investigations, Y.T., V.T.A., R.S., O.B. and H.S.-D. All authors have read and agreed to the published version of the manuscript.

Funding: We acknowledge financial support from the Council of Medical Science, Medical University—Sofia (Contract No. D-109/2024).

Institutional Review Board Statement: The animal study protocol was approved by the Animal Care Ethics Committee of the Bulgarian Agency for Food Safety (BAFS) (protocol code 125 of 7 October 2020) for studies involving animals.

Informed Consent Statement: Not applicable.

Data Availability Statement: All obtained data are presented in this article.

Conflicts of Interest: The authors declare no conflicts of interest.

References

1. WHO. *WHO Consolidated Guidelines on Tuberculosis Module 4: Treatment Drug-Susceptible Tuberculosis Treatment*; World Health Organization: Geneva, Switzerland, 2022.
2. Ghiano, D.G.; Recio-Balsells, A.; Bortolotti, A.; Defelipe, L.A.; Turjanski, A.; Morbidoni, H.R.; Labadie, G.R. New one-pot synthesis of anti-tuberculosis compounds inspired on isoniazid. *Eur. J. Med. Chem.* **2020**, *208*, 112699. [CrossRef] [PubMed]
3. Ghiya, S.; Joshi, Y.C. Synthesis and antimicrobial evaluation of hydrazones derived from 4-methylbenzenesulfonohydrazide in aqueous medium. *Med. Chem. Res.* **2016**, *25*, 970–976. [CrossRef]
4. Mascarello, A.; Mori, M.; Chiaradia-Delatorre, L.D.; Menegatti, A.C.O.; Monache, F.D.; Ferrari, F.; Yunes, R.A.; Nunes, R.J.; Terenzi, H.; Botta, B.; et al. Discovery of Mycobacterium tuberculosis Protein Tyrosine Phosphatase B (PtpB) Inhibitors from Natural Products. *PLoS ONE* **2013**, *8*, e77081. [CrossRef] [PubMed]
5. Navakoski de Oliveira, K.; Chiaradia, L.D.; Alves Martins, P.G.; Mascarello, A.; Sechini Cordeiro, M.N.; Carvalho Guido, R.V.; Andricopulo, A.D.; Yunes, R.A.; Nunes, R.J.; Vernal, J.; et al. Sulfonyl-hydrazones of cyclic imides derivatives as potent inhibitors of the Mycobacterium tuberculosisprotein tyrosine phosphatase B (PtpB). *MedChemComm* **2011**, *2*, 500–504. [CrossRef]
6. Bhat, M.; Poojary, B.; Kumar, S.M.; Hussain, M.M.; Pai, N.; Revanasiddappa, B.; Kullaiah, B. Structural, crystallographic, Hirshfeld surface, thermal and antimicrobial evaluation of new sulfonyl hydrazones. *J. Mol. Struct.* **2018**, *1159*, 55–66. [CrossRef]
7. Ozmen, U.O.; Olgun, G. Synthesis, characterization and antibacterial activity of new sulfonyl hydrazone derivatives and their nickel(II) complexes. *Spectrochim. Acta A Mol. Biomol. Spectrosc.* **2008**, *70*, 641–645. [CrossRef] [PubMed]
8. Popiołek, Ł. The bioactivity of benzenesulfonyl hydrazones: A short review. *Biomed. Pharmacother.* **2021**, *141*, 111851. [CrossRef] [PubMed]
9. Siemann, S.; Evanoff, D.P.; Marrone, L.; Clarke, A.J.; Viswanatha, T.; Dmitrienko, G.I. N-arylsulfonyl hydrazones as inhibitors of IMP-1 metallo-beta-lactamase. *Antimicrob. Agents Chemother.* **2002**, *46*, 2450–2457. [CrossRef] [PubMed]
10. Angelova, V.T.; Pencheva, T.; Vassilev, N.; K-Yovkova, E.; Mihaylova, R.; Petrov, B.; Valcheva, V. Development of New Antimycobacterial Sulfonyl Hydrazones and 4-Methyl-1,2,3-thiadiazole-Based Hydrazone Derivatives. *Antibiotics* **2022**, *11*, 562. [CrossRef]
11. Valcheva, V.; Simeonova, R.; Mileva, M.; Philipov, S.; Petrova, R.; Dimitrov, S.; Georgieva, A.; Tsvetanova, E.; Teneva, Y.; Angelova, V.T. In Vivo Toxicity, Redox-Modulating Capacity and Intestinal Permeability of Novel Aroylhydrazone Derivatives as Anti-Tuberculosis Agents. *Pharmaceuticals* **2022**, *15*, 79. [CrossRef]
12. Teneva, Y.; Simeonova, R.; Valcheva, V.; Angelova, V.T. Recent Advances in Anti-Tuberculosis Drug Discovery Based on Hydrazide-Hydrazone and Thiadiazole Derivatives Targeting InhA. *Pharmaceuticals* **2023**, *16*, 484. [CrossRef] [PubMed]
13. Europe Co. (Ed.) *European Convention for the Protection of Vertebrate Animals Used for Experimental and Other Scientific Purposes (ETS 123)*; Council of Europe: Strasbourg, France, 1991.
14. Lorke, D. A new approach to practical acute toxicity testing. *Arch. Toxicol.* **1983**, *54*, 275–287. [CrossRef]
15. Chinedu, E.; Arome, D.; Ameh, F.S. A new method for determining acute toxicity in animal models. *Toxicol. Int.* **2013**, *20*, 224–226. [CrossRef]

16. Chen, C.; Wicha, S.G.; de Knegt, G.J.; Ortega, F.; Alameda, L.; Sousa, V.; de Steenwinkel, J.E.M.; Simonsson, U.S.H. Assessing Pharmacodynamic Interactions in Mice Using the Multistate Tuberculosis Pharmacometric and General Pharmacodynamic Interaction Models. *CPT Pharmacomet. Syst. Pharmacol.* **2017**, *6*, 787–797. [CrossRef] [PubMed]
17. Lillie, R.D. STUDIES ON HISTOCHEMICAL ACYLATION PROCEDURES. I. PHENOLS. *J. Histochem. Cytochem.* **1964**, *12*, 522–529. [CrossRef]
18. Polizio, A.H.; Peña, C. Effects of angiotensin II type 1 receptor blockade on the oxidative stress in spontaneously hypertensive rat tissues. *Regul. Pept.* **2005**, *128*, 1–5. [CrossRef]
19. Bump, E.A.; Taylor, Y.C.; Brown, J.M. Role of glutathione in the hypoxic cell cytotoxicity of misonidazole. *Cancer Res.* **1983**, *43*, 997–1002. [PubMed]
20. Aebi, H. [13] Catalase in vitro. *Methods Enzymol.* **1984**, *105*, 121–126.
21. Chetty, S.; Armstrong, T.; Kharkwal, S.S.; Drewe, W.C.; De Matteis, C.I.; Evangelopoulos, D.; Bhakta, S.; Thomas, N.R. New InhA Inhibitors Based on Expanded Triclosan and Di-Triclosan Analogues to Develop a New Treatment for Tuberculosis. *Pharmaceuticals* **2021**, *14*, 361. [CrossRef]
22. Doğan, H.; Doğan, D.; Gündüz, M.G.; Krishna, V.S.; Lherbet, C.; Sriram, D.; Şahin, O.; Sarıpınar, E. Discovery of hydrazone containing thiadiazoles as Mycobacterium tuberculosis growth and enoyl acyl carrier protein reductase (InhA) inhibitors. *Eur. J. Med. Chem.* **2020**, *188*, 112035. [CrossRef]
23. Doğan, Ş.D.; Gündüz, M.G.; Doğan, H.; Krishna, V.S.; Lherbet, C.; Sriram, D. Design and synthesis of thiourea-based derivatives as Mycobacterium tuberculosis growth and enoyl acyl carrier protein reductase (InhA) inhibitors. *Eur. J. Med. Chem.* **2020**, *199*, 112402. [CrossRef]
24. Bruker, A. *APEX 2. Bruker Advanced X-ray Solutions*; Bruker: Madison, WI, USA, 2004.
25. Bruker, A. *Saint and SADABS*; Bruker AXS Inc.: Madison, WI, USA, 2009.
26. Sheldrick, G.M. SHELXT–Integrated space-group and crystal-structure determination. *Acta Crystallogr. Sect. A Found. Adv.* **2015**, *71*, 3–8. [CrossRef] [PubMed]
27. Cunha, M.R.; Tavares, M.T.; Carvalho, C.F.; Silva, N.A.T.; Souza, A.D.F.; Pereira, G.J.V.; Ferreira, F.F.; Parise-Filho, R. Environmentally safe condition for the synthesis of aryl and alkyl sulfonyl hydrazones via one-pot reaction. *ACS Sustain. Chem. Eng.* **2016**, *4*, 1899–1905. [CrossRef]
28. Ozochukwu, I.S.; Okpareke, O.C.; Izuogu, D.C.; Ibezim, A.; Ujam, O.T.; Asegbeloyin, J.N. N′-(Pyridin-3-ylmethylene) benzenesulfonohydrazide: Crystal structure, DFT, Hirshfeld surface and in silico anticancer studies. *Eur. J. Chem.* **2021**, *12*, 256–264. [CrossRef]
29. Rahman, M.M.; Hussain, M.M.; Arshad, M.N.; Awual, M.R.; Asiri, A.M. Arsenic sensor development based on modification with (E)-N′-(2-nitrobenzylidine)-benzenesulfonohydrazide: A real sample analysis. *New J. Chem.* **2019**, *43*, 9066–9075. [CrossRef]
30. Blatova, O.A.; Asiri, A.M.; Al-Amshany, Z.M.; Arshad, M.N.; Blatov, V.A. Molecular packings and specific-bonding patterns in sulfonamides. *New J. Chem.* **2014**, *38*, 4099–4106. [CrossRef]
31. Hodge, H.C.; Sterner, J.H. Tabulation of Toxicity Classes. *Am. Ind. Hyg. Assoc. Q.* **1949**, *10*, 93–96. [CrossRef]
32. Ogawa, K.; Ito, M. Appetite-enhancing Effects of trans-Cinnamaldehyde, Benzylacetone and 1-Phenyl-2-butanone by Inhalation. *Planta Med.* **2016**, *82*, 84–88. [CrossRef]
33. Niedernhofer, L.J.; Daniels, J.S.; Rouzer, C.A.; Greene, R.E.; Marnett, L.J. Malondialdehyde, a Product of Lipid Peroxidation, Is Mutagenic in Human Cells. *J. Biol. Chem.* **2003**, *278*, 31426–31433. [CrossRef]
34. Bains, V.K.; Bains, R. The antioxidant master glutathione and periodontal health. *Dent. Res. J.* **2015**, *12*, 389–405. [CrossRef]
35. Chen, Y.; Dong, H.; Thompson, D.C.; Shertzer, H.G.; Nebert, D.W.; Vasiliou, V. Glutathione defense mechanism in liver injury: Insights from animal models. *Food Chem. Toxicol.* **2013**, *60*, 38–44. [CrossRef] [PubMed]
36. Nair, A.; Sharma, P.; Tiwary, M.K. Glutathione deficiency in COVID19 illness-does supplementation help? *Saudi J. Anaesth.* **2021**, *15*, 458–460. [CrossRef] [PubMed]
37. Nandi, A.; Yan, L.J.; Jana, C.K.; Das, N. Role of Catalase in Oxidative Stress- and Age-Associated Degenerative Diseases. *Oxid. Med. Cell. Longev.* **2019**, *2019*, 9613090. [CrossRef] [PubMed]